Solution-Processed Small-Molecule Bulk Heterojunction Ambipolar Transistors

Shiau-Shin Cheng, Peng-Yi Huang, Mohan Ramesh, Hsiu-Chieh Chang, Li-Ming Chen, Chia-Ming Yeh, Chun-Lin Fung, Meng-Chyi Wu, Chung-Chi Liu, Choongik Kim, Hong-Cheu Lin, Ming-Chou Chen,* and Chih-Wei Chu**

Solution-processed small-molecule bulk heterojunction (BHJ) ambipolar organic thin-film transistors are fabricated based on a combination of [2-phenylbenzo[*d*,*d*']thieno[3,2-*b*;4,5-*b*']dithiophene (P-BTDT) : 2-(4-*n*-octylphenyl)benzo[*d*,*d*']thieno[3,2-*b*;4,5-*b*']dithiophene (OP-BTDT)] and C_{60}. Treating high electrical performance vacuum-deposited P-BTDT organic semiconductors with a newly developed solution-processed organic semiconductor material, OP-BTDT, in an optimized ratio yields a solution-processed *p*-channel organic semiconductor blend with carrier mobility as high as 0.65 $cm^2 V^{-1} s^{-1}$. An optimized blending of P-BTDT:OP-BTDT with the *n*-channel semiconductor, C_{60}, results in a BHJ ambipolar transistor with balanced carrier mobilities for holes and electrons of 0.03 and 0.02 $cm^2 V^{-1} s^{-1}$, respectively. Furthermore, a complementary-like inverter composed of two ambipolar thin-film transistors is demonstrated, which achieves a gain of 115.

1. Introduction

Organic thin-film transistors (OTFTs) have attracted much attention due to their potential applications in high-value, low-cost electronic devices, including displays, sensors, radio-frequency identification components, and e-papers.[1–3] Current research in OTFT materials is focused primarily on the design and synthesis of conjugated organic compounds and polymers that are environmentally stable and capable of carrier transport. Several conjugated organic compounds and polymers have been developed with promising carrier mobilities, comparable to that of amorphous silicon.[4–6] To exploit such materials in a wider range of practical applications, high-performance inverters, which are the building blocks of integrated circuits (ICs), must be developed. Complementary metal-oxide semiconductor (CMOS) technology is desirable for the preparation of ICs because it provides straightforward circuit design, good noise margins, low power consumption, and robust operation. Organic CMOS technology requires the use of p- and n-type transistors on the same substrate; however, the separate vacuum-deposition of p- and n-type semiconductors increases the complexity of the circuit fabrication process.[7,8] To overcome this problem, researchers have explored several strategies, including: i) ambipolar OTFTs featuring symmetric or asymmetric source and drain electrodes for single organic semiconductors;[9–12] ii) bilayer structures consisting of hole- and electron-transporting organic compounds;[13–16] and iii) blending two organic semiconductors with different polarities to eliminate the need to pattern the p- and n-channel semiconductors in separation regions.[17–20]

In a single-material configuration, the efficient injection of both holes and electrons is the key factor affecting the performance of ambipolar OTFTs. Improved carrier mobility can be achieved by lowering the barrier between the energy levels of the metal and those of the highest occupied molecular orbital (HOMO) of the organic semiconductor for hole transport, and of the lowest unoccupied molecular orbital (LUMO) for electron transport. Most organic semiconductors have a wide band gap (ca. 2–3 eV), resulting in a mismatch between the work function of the electrode and the organic semiconductor for at least one of the carriers. Although devices featuring asymmetric electrodes could circumvent this drawback, the preparation of such a device demands an additional deposition step. Therefore, several research groups have investigated the use of a bilayer structure, with carrier mobility of electrons and holes reaching as

Prof. C. Kim
Department of Chemical and Biomolecular Engineering
Sogang University
1 Shinsoo-dong, Mapo-gu, Seoul, Korea, 121742
E-mail: choongik@sogang.ac.kr
Prof. C.-W. Chu
Research Center for Applied Sciences
Academia Sinica, Taipei 115, Taiwan
Department of Photonics
National Chiao Tung University
Hsinchu 300, Taiwan (ROC)
E-mail: gchu@gate.sinica.edu.tw
S.-S. Cheng, L.-M. Chen, C.-L. Fung, Dr. M.-C. Wu
Institute of Electronics Engineering
National Tsing Hua University
Hsinchu, 300, Taiwan (ROC)
Dr. P.-Y. Huang, H.-C. Chang C.-M. Yeh, C.-C. Liu, Prof. M.-C. Chen
Department of Chemistry
National Central University
Jhong-Li, 320, Taiwan (ROC)
E-mail: mcchen@ncu.edu.tw
M. Ramesh, Dr. H.-C. Lin
Department of Materials Science and Engineering
National Chiao Tung University
Hsinchu, 300, Taiwan (ROC)

DOI: 10.1002/adfm.201303378

high as 10^{-1} cm^2 V^{-1} s^{-1}.[21,22] Bilayer structures based on solution-processed organic semiconductors are challenging to fabricate, due to the dissolution of the initial layer by subsequent layers deposited during spin-coating, making multilayer spin-coated films difficult to exploit. Therefore, bulk heterojunction (BHJ) structures appear to be the most promising for device fabrication, as they are readily deposited using a single solution process.[17] Unfortunately, carrier mobilities in these devices rarely exceed the order of 10^{-2} cm^2 V^{-1} s^{-1} because of poor control over molecular packing and orientation in these blend systems, with a few exceptions.[23,24] Therefore, in order to achieve high-performance ambipolar OTFTs featuring BHJ structures, there is a need to develop soluble p- and n-type organic semiconductors with strong π-stacking behavior. Among solution-processable organic semiconductors, small molecules exhibit certain advantages over polymeric materials as demonstrated in this study, although polymeric materials are considered to be better in terms of processability. Compared to polymeric materials, small molecule materials are easier to synthesize and purify, which greatly improve reproducibility of fabricated devices. Small molecules can easily be purified by various methods of chromatography, sublimation, and recrystallization, while polymers can only be purified by recrystallization. Furthermore, due to molecular weight distribution (polydispersity), regio- and stereo- irregularity, and end-group contaminations of polymeric materials, performance of polymer-based OTFTs could exhibit relatively large batch-to-batch variations.

Carrier transport between individual organic units is strongly dependent on the molecular ordering. Research efforts are therefore typically directed towards the development of chemically stable π-conjugated planar structures. Unfortunately, highly π-conjugated systems, such as oligoacenes and thiophenes, usually have low solubility in organic solvents due to their strong intermolecular interactions, which leads to the nucleation of molecular crystals in solution. To enhance the solubility of oligoacenes, Anthony et al. disrupted the edge-to-face and face-to-face interactions by appending triisopropylsilyl (TIPS) groups at the C6 and C13 positions of pentacene, resulting in increased π-overlap and decreased interplanar separation.[25,26] Unfortunately, the TIPS-pentacene derivative underwent rapid degradation due to photoinduced oxidative decomposition, with the formation of dimeric Diels–Alder adducts at the electron-rich central ring.[27,28] Recently, many research groups have reported that the presence of fused thiophene units in π-conjugated oligomers is an effective means of invoking strong intermolecular interactions and improving environmental stability.[29–33] Youn et al. demonstrated OTFTs with promising characteristics (*e.g.*, mobilities as high as 0.7 cm^2 V^{-1} s^{-1}) when employing fused thiophene derivatives such as 2-phenylbenzo[*d*,*d*']thieno[3,2-*b*;4,5-*b*']dithiophene (P-BTDT).[34] However, film deposition by thermal evaporation was necessary for P-BTDT due to the compounds having poor solubility in organic solvents.

To take advantage of the versatile chemical modification of fused thiophene,[35–37] we synthesized a new soluble BTDT derivative, 2-(4-*n*-octylphenyl)benzo[*d*,*d*']thieno[3,2-b;4,5-b;'] dithiophene (OP-BTDT). Via a spin-coating solution process, OP-BTDT-based OTFT exhibited a moderate field-effect hole mobility of 0.05 cm^2 V^{-1} s^{-1}. Recently, solution-processed organic transistors based on semiconductor blends have been explored, revealing the advantageous properties of their individual components.[34] We followed a similar strategy in this study, taking advantage of the good transistor performance and the thermal and photooxidative stability of P-BTDT, and the excellent solubility of OP-BTDT in OTFTs. We have demonstrated that, by blending appropriate amounts of P-BTDT and OP-BTDT (denoted as M-BTDT in this study), the mobility can be increased by one order of magnitude, up to 0.65 cm^2 V^{-1} s^{-1}. Encouraged by such excellent mobility via a solution process, we have also explored solution-processable small-molecule BHJ ambipolar transistors based on blends of M-BTDT (P-BTDT:OP-BTDT) and C_{60}. For a suitable weight ratio of M-BTDT and C_{60}, we optimized the device to achieve a finely structured network of the materials with two different phases and balanced hole (0.03 cm^2 V^{-1} s^{-1}) and electron (0.02 cm^2 V^{-1} s^{-1}) mobilities. Finally, we developed an integrated organic inverter featuring two of these identical ambipolar transistors, which achieved a transfer gain of 115.

2. Results and Discussion

The chemical structures of OP-BTDT and P-BTDT and the device structure are presented in **Figure 1**(a); detailed synthetic procedures are provided in the experimental section. Differential pulse voltammetry (DPV) was performed on the BTDT derivatives in dichlorobenzene (DCB) at 25 °C. The DPV trace exhibited an oxidation peak at +1.33 V and a reduction peak at –1.93 V (using ferrocene/ferrocenium as the internal standard at +0.6 V), which is consistent with previously reported results for P-BTDT.[34] The electrochemically derived HOMO–LUMO energy gap of these two BTDTs, obtained from the DPV traces, is 3.26 eV, with a HOMO energy level for both BTDTs near –5.53 eV, significantly lower than that of pentacene (–5.14 eV; assuming ferrocene/ferrocenium oxidation at –4.8 eV). The combination of large band gap and relatively low HOMO energy level suggests that the corresponding BTDT derivatives are environmentally stable.

A typical TFT based on solution-processed OP-BTDT film exhibited carrier mobility of 0.05 cm^2 V^{-1} s^{-1} (Figure S1, Supporting Information). To achieve high mobility and good environmental stability along with high solubility, we selected P-BTDT as a blending material because of its greater crystallinity than that of OP-BTDT. Indeed, we found that the solubility of P-BTDT was enhanced dramatically when blended with OP-BTDT, presumably because of π–π interactions between their BTDT core structures. OP-BTDT can, therefore, be considered to play the role of a surfactant that increases the solubility of P-BTDT. To investigate and optimize blending ratios of OP-BTDT and P-BTDT on the electrical performance of the resulting TFTs, we have varied blending ratios of OP-BTDT to P-BTDT from 1:0 (pure OP-BTDT) to 1:0.50 (**Table 1**). The highest carrier mobility was achieved at a ratio of 1:0.33; Figure 1(b) displays the corresponding device characteristics. The mobility of 0.65 cm^2 V^{-1} s^{-1} is close to that of pure P-BTDT film fabricated via thermal evaporation.[34] Furthermore, to investigate the molecular packing structures of blend thin films and correlate them with device performance, we have

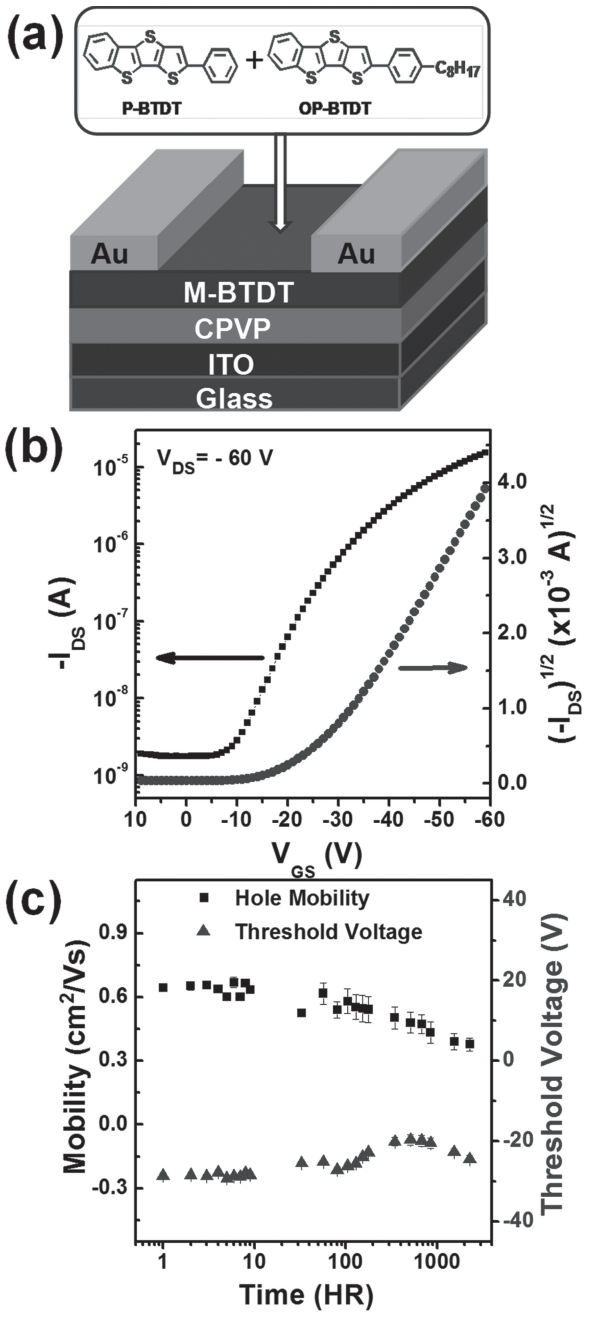

Figure 1. (a) Schematic of the device configuration employed in this study, with chemical structures of the small molecules OP-BTDT and P-BTDT. (b) Transfer characteristics of an M-BTDT (P-BTDT:OP-BTDT = 1:0.33) OTFT. (c) Environmental stability of an M-BTDT (P-BTDT:OP-BTDT = 1:0.33) OTFT.

performed XRD analysis of OP-BTDT and M-BTDT thin films (Figures S3-S4). As shown in Figure S3A, pure OP-BTDT film showed multiple Bragg reflections at different positions from those of P-BTDT film,[34] possibly due to different film microstructure originated from n-octyl chain. On the other hand, for M-BTDT (with different OP-BTDT:P-BTDT ratios) films, a few peaks disappeared or showed little peak intensities, and peak positions are a bit shifted compared to pure OP-BTDT

Table 1. Device performance of OTFTs prepared with different OP-BTDT:P-BTDT ratios; V_{DS} and V_{GS} were both set at –60 V

OP-BTDT:P-BTDT ratio	Mobility [$cm^2 V^{-1} s^{-1}$]	Threshold voltage [V]	Current on/off ratio
pure OP-BTDT	0.05	–29.7	10^4
1:0.20	0.28	–22.2	10^3
1:0.33	0.65	–28.6	10^4
1:0.50	0.17	–26.2	10^4
pure P-BTDT[a)]	0.70	–4.1	10^8 3[4]

[a)]Vapor-deposited onto the octadecyltrichlorosilane-treated Si/SiO_2 substrate.

film (Figures S3B-D). If we assign the first peak (2θ = 4.4°) of OP-BTDT film as (001) reflection, the corresponding d-spacing value is 20.1 Å, slightly smaller than molecular length (23.0 Å) of OP-BTDT. Calculated tilt angle of OP-BTDT molecules in the film is approximately 61°. On the other hand, d-spacing values of M-BTDT films (2θ = 3.7–3.9°) are 22.6–23.8 Å, which indicates that molecules are more predominantly aligned with their long molecular axis along the surface normal with tilt angles of 80 – 90°, compared to OP-BTDT films. Note that P-BTDT molecules showed similar molecular alignment with tilt angle ~90°; molecular arrangement of P-BTDT might facilitate the favorable film microstructure of M-BTDT films for higher device performance.[34] Based on XRD data, we propose molecular arrangements of OP-BTDT and M-BTDT (Figure S4), which elucidate higher device performance of M-BTDT film (carrier mobility of 0.17–0.65 $cm^2 V^{-1} s^{-1}$) than that of OP-BTDT (0.05 $cm^2 V^{-1} s^{-1}$). Particularly, M-BTDT film with OP-BTDT:P-BTDT ratio of 1:0.33 showed a bit more Bragg reflections with higher intensities (Figure S3C) compared to other blend films, which indicate better film crystallinity leading to the highest device performance (Table 1).

In addition to high electrical device performance, air stability is another significant factor for many OTFT applications. To test their stability, we exposed freshly fabricated devices to air and periodically measured their performance. Figure 1(c) shows that both the hole mobility and threshold voltage remained constant for the first 100 h, with slight fluctuations within the period from 100 to 1000 h. Similarly, transistor off-current was also monitored as a function of time. As shown in Figure S5, off-current showed only slight fluctuation between 10^{-9} and 10^{-8} A up to ~2500 h.

In a previous study, we discovered that C_{60}-based transistors exhibiting reasonable electron mobilities could be obtained through solution processing.[6] Therefore, in this study, we also used solution processing to fabricate small-molecule BHJ ambipolar transistors based on blends of OP-BTDT and P-BTDT (M-BTDT) with C_{60}. Metallic Au was selected as the source and drain (S/D) electrode material. The device energy level diagram of M-BTDT/C_{60} blends is shown in **Figure 2**a. The energy levels are shown as straight lines for simplicity. When the gate bias is applied, band bending occurs at the semiconductor/dielectric interface, resulting in band bending at the electrode/semiconductor interface.[38] We expected that varying the M-BTDT to C_{60} weight ratio would influence the transport pathways and their crystallinity for hole and electron transport. Figure 2(b)

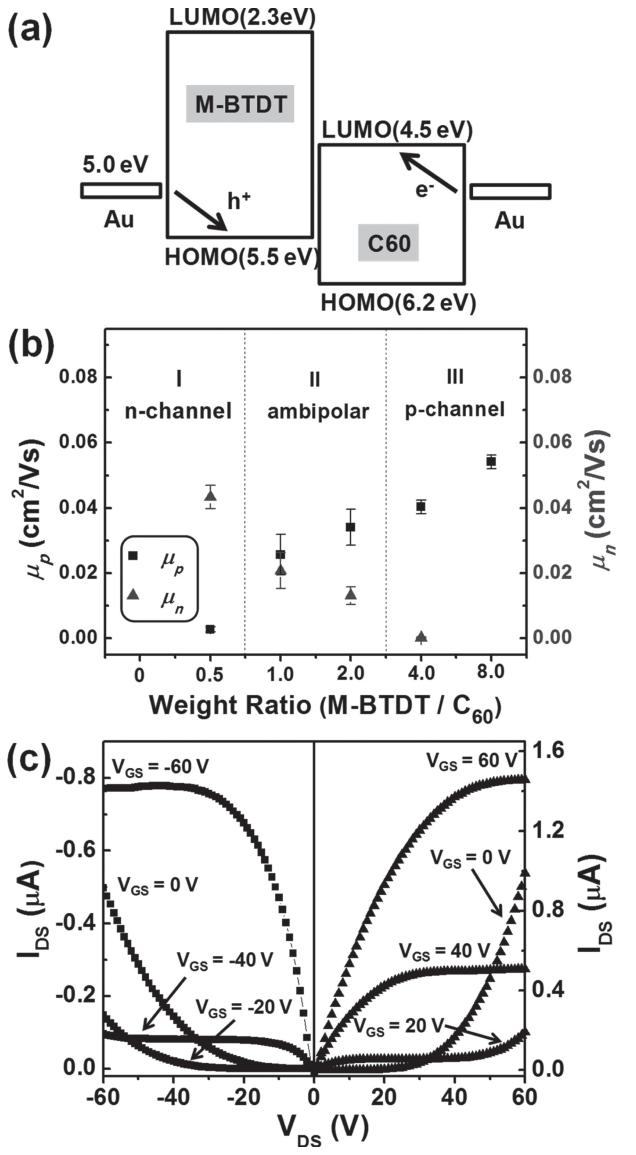

Figure 2. (a) Device energy level diagram of M-BTDT/C_{60} blends with Au electrodes, when no biases are applied to the transistor. (b) Hole (■) and electron (▲) mobilities in BHJ ambipolar OTFTs, plotted with respect to the M-BTDT to C_{60} weight ratio. The BHJ devices operated in three models: n-channel (regime I), ambipolar (regime II), and p-channel (regime III). (c) Output characteristics of an ambipolar OTFT featuring a BHJ with an M-BTDT to C_{60} weight ratio of 1:1, operated under both positive and negative biases.

displays the hole (μ_p) and electron (μ_e) mobilities of devices with different M-BTDT to C_{60} weight ratios. Depending on the weight ratio, these devices exhibited three operating modes: (I) an n-channel regime (where a larger amounts of n-type materials occupied the channel regime, *vide infra*), (II) an ambipolar transport regime (where both the n- and p-type materials equally filled the channel regime), and (III) a p-channel regime (where a larger amount of p-type materials occupied the channel regime). For devices with M-BTDT to C_{60} weight ratios of less than 0.5, the mobility of electrons was one order of magnitude higher than that of holes. In regime I, we suspect that the device possesses more electron pathways than hole pathways; i.e., n-type materials occupy the majority of the channel. Therefore, n-type unipolar transport characteristics dominate. Furthermore, the electron mobility in the BHJ transistor was close to that of single-layer C_{60} devices.[6] Further increasing the M-BTDT to C_{60} weight ratio caused the p-channel pathway to increase at the expense of the n-channel pathway. As a result, the hole mobility was increased marginally.

Interactions between M-BTDT and C_{60} could lead to recombination, such that the n-type behavior is only partially inhibited, rather than totally sacrificed. Notably, we observed ambipolar behavior only at ratios of 1.0, 2.0, and 4.0, as revealed in regimes II and III. When the M-BTDT to C_{60} weight ratio in the BHJ transistor was between 1.0 and 4.0, the mobility of the electrons and holes was balanced and the device exhibited the ambipolar transport behavior of regime II, as shown in Figure 2(b). An M-BTDT to C_{60} ratio of 1.0 was found to be optimum for the balanced mobility of holes and electrons. A further increase in the M-BTDT to C_{60} weight ratio to greater than 1.0 led to more p-type material in the channel, resulting in a weakening of the balanced ambipolar conditions. When the M-BTDT to C_{60} weight ratio was 4.0 or greater, the device exhibited the p-type unipolar transport characteristics of regime III, as shown in Figure 2(b). Taken together, these results suggest that when the BHJ ambipolar transistor features an optimized weight ratio of p- and n-type small-molecule materials, the mobilities for holes and electron are balanced.

Figures 2(c) shows output characteristics of a BHJ ambipolar transistor incorporating M-BTDT and C_{60} at a weight ratio of 1.0. This device exhibited strong field-effect modulations of channel conductance during ambipolar operation, with carrier mobilities (μ) for holes and electrons of 0.03 and 0.02 $cm^2\ V^{-1}\ s^{-1}$, respectively. Figure 2(c) reveals the ambipolar characteristics of this sample in both electron- and hole-enhancement modes. At low values of V_{GS}, the BHJ ambipolar transistor exhibited diode-like curves, which are frequently observed for typical ambipolar transistors,[9,10,39] due to the presence of both charge carriers in the channel of the device. We attribute this behavior to the highly negative value of V_T for p-channel operation and/or the positive threshold voltage for n-channel operation. The relatively high threshold voltages imply electron and hole trapping at the interface between the p- and n-type organic materials in the phase-separated network (Table 1).[40]

To further investigate the degree of charge trapping, we extracted the sub-threshold slope (SS) using the equation:

$$SS = (d \log IDS / d \log VGS)^{-1}$$

with the corresponding density of traps (N_{SS}) given by the approximation:

$$N_{SS} = (SS \log e/(kT/q) - 1)(C_i/q)$$

where k is Boltzmann's constant, T is the absolute temperature, and q is the charge of an electron. The values of SS of the p- and n-channels were 22.17 and 27.09 V decade^{-1}, respectively; the corresponding values of N_{SS} were 1.14×10^{13} and 1.4×10^{13} cm^{-2}, respectively. Because the values of SS for the

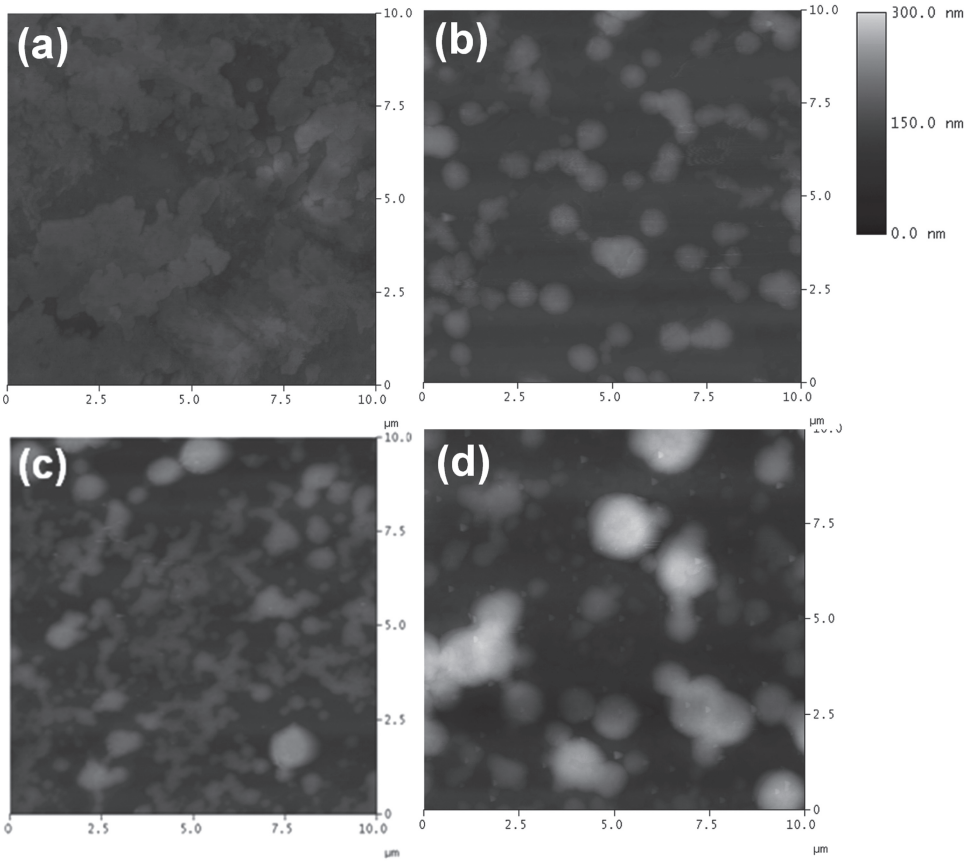

Figure 3. AFM images (10 μm × 10 μm) of (a) pure M-BTDT and (b–d) M-BTDT/C_{60} blends with weight ratios of (b) 4.0, (c) 2.0, and (d) 1.0.

p- and n-channels were larger than the theoretical minimum of 58 meV decade^{-1} [kT/q ln (10)], the larger density of traps for holes and electrons would result in larger values of V_T in the BHJ ambipolar transistors.

We used AFM to determine the reason behind the ambipolar behavior of the BHJ ambipolar transistors, and to investigate whether the M-BTDT to C_{60} weight ratio had any influence on the phase-separated network. **Figure 3**(a) displays AFM image of the pure M-BTDT film; Figures 3(b)–(d) present AFM images of the M-BTDT/C_{60} films at weight ratios of 4.0, 2.0, and 1.0, respectively. Two distinct phases appear in Figures 3(b)–(d), with the number and size of one material increasing upon decreasing the M-BTDT to C_{60} weight ratio; the light regions represent the C_{60} phase. When the M-BTDT to C_{60} weight ratio is 1.0, Figure 3(d) shows that more of the C_{60} phase was present in larger-sized particles within a two-phase discontinuous network structure. These larger particles of the C_{60} phase balanced carrier mobilities of the holes and electrons (vide supra), as we had observed in Figure 2(a). Increasing the M-BTDT to C_{60} ratio to 2.0 (Figure 3(c)) or 4.0 (Figure 3(b)) decreased the particle size of the C_{60} phase and disrupted the ambipolar behavior by increasing the p-channel characteristics.

The BHJ ambipolar transistors described herein are suitable for fabrication using CMOS technology. We prepared an inverter as a CMOS device feasibility study. Inverters are an essential logic cell building block in ICs. **Figure 4** displays the transfer characteristics of CMOS-like inverters based on two identical BHJ ambipolar transistors; the inset displays an equivalent circuit of the inverter. Because of its unique ambipolar characteristics, the inverter was capable of operating in both positive and negative V_{IN} and V_{DD}. We calculated the different transfer gains of the inverter at different supply voltages (V_{DD}). The transfer gain is defined as dV_{OUT}/dV_{IN}, where V_{OUT} and V_{IN} are the output and input voltages, respectively. At positive V_{IN} and V_{DD} (70 V), the inverter exhibited a maxium transfer gain of 83. On the other hand, at negative V_{IN} and V_{DD} (–70 V), the inverter showed a maximum transfer gain of 115.

3. Conclusion

We have synthesized a new soluble BTDT-based fused-thiophene derivative for the preparation of BHJ ambipolar transistors through solution processing. Different blending ratios of M-BTDT to C_{60} resulted in the formation of different phase-separated networks and three operational regimes. At an optimized M-BTDT to C_{60} weight ratio, the device exhibited a finely structured transport network with balanced hole and electron mobilities. By employing the BHJ ambipolar transistors as active layers in a CMOS device, an inverter with a large transfer gain of 115 was acheived.

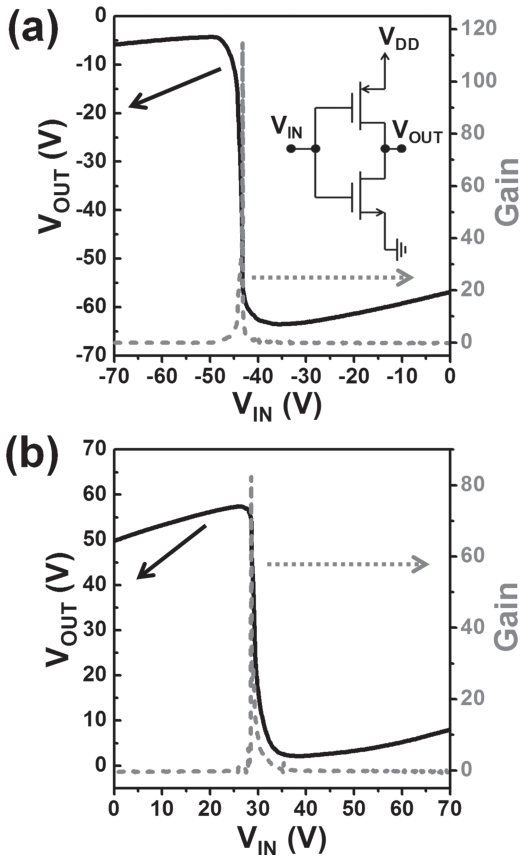

Figure 4. Transfer characteristics of CMOS-like inverters comprised of two identical BHJ ambipolar thin-film transistors (1:1 weight ratio of M-BTDT:C_{60}); (a) Inverter characteristics and gain at negative V_{IN} and V_{DD} (–70 V). Inset shows the inverter circuit diagram. (b) Inverter characteristics and gain at positive V_{IN} and V_{DD} (70 V).

4. Experimental Section

Materials and Methods: All chemicals and solvents were obtained in reagent grade from Aldrich, Arco, and TCI Chemical. Toluene, benzene, ether, and THF were distilled under N_2 from Na/benzophenone ketyl; halogenated solvents were distilled from CaH_2. For the preparation of BTDT, NMR spectra, and DPV (differential pulse voltammogram) experiments, we have followed experimental procedures from the literature.[34]

2-(4-n-Octylphenyl)benzo[d,d´]thieno[3,2-b;4,5-b´]dithiophene (OP-BTDT): Under N_2 and anhydrous conditions at 0 °C, 2.5 M *n*-BuLi (0.810 mL in hexanes, 2.03 mmol) was added slowly to a solution of BTDT (500 mg, 2.03 mmol) in THF (40 mL) and then the mixture was stirred for 40 min. Next, tri-*n*-butyltin chloride (0.63 mL, 2.23 mmol) was added and the mixture, which was then stirred for 30 min at this temperature before warming to room temperature and stirring overnight. After simple filtration, the solvent was evaporated under vacuum and toluene (30 mL) was added. The resulting solution was added to a solution of 1-bromo-4-*n*-octylbenzene (0.500 mL, 2.23 mmol) and tetrakis(triphenylphosphine)palladium (94 mg, 0.08 mmol) in toluene (30 mL) and then the mixture was heated under reflux for 2 days. The precipitate was filtered off and washed with hexanes to giving a bright-yellow solid (509 mg, 84%). Further purification of OP-BTDT was performed through recrystallization and gradient sublimation under a pressure of approximately 10^{-5} torr. ^{1}H NMR ($CDCl_3$, 300 MHz): δ 7.87 (d, *J* = 8.1 Hz, 1H), 7.82 (d, *J* = 8.1 Hz, 1H), 7.57 (d, *J* = 8.1 Hz, 2H in OP), 7.53 (s, 1H), 7.43 (t, *J* = 7.8 Hz, 1H), 7.35 (t, *J* = 7.8 Hz, 1H), 7.24 (d, *J* = 8.1 Hz, 2H in OP), 2.64 (t, *J* = 7.5 Hz, 2H), 1.63 (m, 2H), 1.33–1.28 (m, 10H), 0.88 (t, *J* = 4,8 Hz, 3H). ^{13}C NMR ($CDCl_3$, 125 MHz): δ 146.70, 143.25, 142.37, 141.79, 135.92, 133.73, 133.03, 130.49, 130.04, 129.12, 125.83, 125.00, 124.44, 123.98, 120.62, 116.14, 35.74, 31.91, 31.27, 29.49, 29.35, 29.25, 22.65, 14.00. Anal. Calcd for $C_{26}H_{26}S_3$: C, 71.84; H, 6.03; Found: C, 71.77; H, 6.09. HRMS (EI, *m*/*z*) calcd.: 434.1197 (M^+); found: 434.1195.

BHJ Ambipolar Transistors: The devices were fabricated on ITO-coated glass substrates, which were used as the gate electrode. After routine solvent cleaning, the substrates were treated with UV–ozone for 25 min. The cleaned ITO substrates were then covered with a 700-nm-thick polymer dielectric insulator, prepared by spin-coating a solution of poly-4-vinylphenol (11 wt%) and poly(melamine-*co*-formaldehyde) (4 wt%) in propylene glycol monomethyl ether acetate. The substrate was then prebaked at 100 °C for 5 min, followed by baking at 200 °C for 20 min, to crosslink the polymer. The resulting film had a capacitance per unit area (C_i) of 4.931 nF cm^{-2}. To study the effect of the transport pathway of the p- and n-type organic semiconductors on the performance of the devices, different weight ratios of the p-type (M-BTDT) and n-type (C_{60}) organic semiconductors were blended in dichlorobenzene and spin-coated onto the gate dielectrics under a N_2 atmosphere inside a glove box. The devices were thermally annealed on the hot plate at 100 °C for 20 min. Finally, Au was thermally evaporated onto the active layer through a shadow mask to form the source and drain electrodes, with the channel width and length of 2000 and 200 μm, respectively. The electrical performance of the devices was measured under an N_2 atmosphere within a glove box using a Keithley 4200 semiconductor parameter analyzer and an HP 4980A Precision LCR meter. AFM images were recorded using a Digital Instruments Nanoscope III apparatus in the tapping mode.

Supporting Information

Supporting Information is available from the Wiley Online Library or from the author.

Acknowledgements

S.-S. Cheng, P.-Y. Huang, and M. Ramesh contributed equally to this work. This work was supported by the National Science Council (NSC) of Taiwan (NSC100-2628-M-008-004 and NSC 101-2113-M008-005), National Tsing-Hua University, Academia Sinica, and by the National Research Foundation of Korea (NRF) grant funded by the Korea government (MSIP) (No. 2011-0007730) and by theCenter for Advanced Soft Electronics under the Global Frontier Research Program of the Ministry of Science, ICT & Future Planning, Korea (Code No. 2013M3A6A5073175).

Received: September 30, 2013
Published online: November 27, 2013

[1] C. D. Sheraw, L. Zhou, J. R. Huang, D. J. Gundlach, T. N. Jackson, *Appl. Phys. Lett.* **2002**, *80*, 1088.
[2] C. J. Drury, C. M. J. Mutsaers, C. M. Hart, M. Matters, D. M. De Leeuw, *Appl. Phys. Lett.* **1998**, *73*, 108.
[3] F. Eder, H. Klauk, M. Halik, U. Zschieschang, G. Schmid, C. Dehm, *Appl. Phys. Lett.* **2004**, *84*, 2673.
[4] Y. Y. Lin, D. J. Gundlach, S. F. Nelson, T. N. Jackson, *IEEE Trans. Electron Devices* **1997**, *44*, 1325.
[5] A. A. Virkar, S. Mannsfeld, Z. Bao, N. Stingelin, *Adv. Mater.* **2010**, *22*, 3857.
[6] C. F. Sung, D. Kekuda, L. F. Chu, Y. Z. Lee, F. C. Chen, M. C. Wu, C. W. Chu, *Adv. Mater.* **2009**, *21*, 4845.

[7] M. S. Oh, K. D. Hwang, K. Lee, *Appl. Phys. Lett.* **2007**, *90*, 173511.
[8] T. Trupke, E. Pink, R. A. Bardos, M. D. Abbott, *Appl. Phys. Lett.* **2007**, *90*, 093506.
[9] T. D. Anthopoulos, D. M. de Leeuw, E. Cantatore, S. Sateyesh, E. J. Meijer, C. Tanase, J. C. Hummelen, P. W. M. Blom, *Appl. Phys. Lett.* **2004**, *85*, 4205.
[10] T. B. Singh, F. Meghdadi, S. Gunes, N. Marjanovic, G. Horowitz, P. Lang, S. Bauer, N. S. Sariciftci, *Adv. Mater.* **2005**, *17*, 2315.
[11] T. D. Anthopoulos, S. Setayesh, E. Smits, M. Cölle, E. Cantatore, B. de Boer, P. W. M. Blom, D. M. de Leeuw, *Adv. Mater.* **2006**, *18*, 1900.
[12] S. Z. Bisri, T. Takenobu, Y. Yomogida, H. Shimotani, T. Yamao, S. Hotta, Y. Iwasa, *Adv. Funct. Mater.* **2009**, *19*, 1728.
[13] A. Dodabalapur, H. E. Katz, L. Torsi, R. C. Haddon, *Science* **1995**, *269*, 1560.
[14] Z. Wei, W. Xu, W. Hu, D. Zhu, *J. Mater. Chem.* **2008**, *18*, 2420.
[15] C. Rost, D. J. Gundlach, S. Karg, W. Riess, *J. Appl. Phys.* **2004**, *95*, 5782.
[16] J. Shi, H. Wang, D. Song, H. Tian, Y. Geng, D. Yan, *Adv. Funct. Mater.* **2007**, *17*, 397.
[17] K. Szendrei, D. Jarzab, Z. Chen, A. Facchetti, M. A. Loi, *J. Mater. Chem.* **2010**, *20*, 1317.
[18] S. Cho, J. Yuen, J. Y. Kim, K. Lee, A. J. Heeger, *Appl. Phys. Lett.* **2006**, *89*, 153505.
[19] L. Chua, J. Zaumseil, J. Chang, E. C. Ou, P. K. Ho, H. Sirringhaus, R. H. Friend, *Nature* **2005**, *434*, 194.
[20] C. Rost, S. Karg, W. Riess, M. A. Lo, M. Murgia, M. Muccini, *Appl. Phys. Lett.* **2004**, *85*, 1613.
[21] J. Shi, H. Wang, D. Song, H. Tian, Y. Geng, D. Yan, *Adv. Funct. Mater.* **2007**, *17*, 397.
[22] M.-J. An, H.-S. Seo, Y. Zhang, J.-D. Oh, J.-H. Choi, *Appl. Phys. Lett.* **2010**, *97*, 023506.
[23] Z. Chen, M. J. Lee, R. S. Ashraf, Y. Gu, S. Albert-Seifried, M. M. Nielsen, B. Schroeder, T. D. Anthopoulos, M. Heeney, I. McCulloch, H. Sirringhaus, *Adv. Mater.* **2012**, *24*, 647.
[24] A. J. Kronemeijer, E. Gili, M. Shahid, J. Rivnay, A. Salleo, M. Heeney, H. Sirringhaus, *Adv. Mater.* **2012**, *24*, 1558.
[25] J. E. Anthony, J. S. Brooks, D. L. Eaton, S. R. Parkin, *J. Am. Chem. Soc.* **2001**, *123*, 9482.
[26] C. D. Sheraw, T. N. Jackson, D. L. Eaton, J. E. Anthony, *Adv. Mater.* **2003**, *15*, 2009.
[27] A. Maliakal, K. Raghavachari, H. Katz, E. Chandross, T. Siegrist, *Chem. Mater.* **2004**, *16*, 4980.
[28] C. Kim, P. Y. Huang, J.-W. Jhuang, M.-C. Chen, J.-Y. Ho, L.-H. Chen, G.-H. Lee, A. Facchetti, T. Marks, *Org. Electron.* **2010**, *11*, 1363.
[29] Y.-Y. Noh, R. Azumi, M. Goto, B.-J. Jung, E. Lim, H.-K. Shim, Y. Yoshida, K. Yase, D.-Y. Kim, *Chem. Mater.* **2005**, *17*, 386
[30] M.-C. Chen, Y.-J. Chiang, C. Kim, Y.-J. Guo, S.-Y Chen, Y.-J. Liang, Y.-W. Huang, T.-S. Hu, G.-H. Lee, A. Facchetti, T. J. Marks, *Chem. Commun.* **2009**, 1846.
[31] C. Kim, M.-C. Chen, Y.-J. Chiang, Y.-J. Guo, J. Youn, H. Huang, Y.-J. Liang, Y.-J. Lin, Y.-W. Huang, T.-S. Hu, G.-H. Lee, A. Facchetti, T. J. Marks, *Org. Electron.* **2010**, *11*, 801.
[32] J. Youn, P.-Y. Huang, Y.-W. Huang, M.-C. Chen, Y.-J. Lin, H. Huang, R. Ponce Ortiz, C. Stern, M.-C. Chung, L.-H. Chen, A. Facchetti, T. J. Marks, *Adv. Funct. Mater.* **2012**, *22*, 48.
[33] Y. M. Sun, Y. W. Ma, Y. Q. Liu, Y. Y. Lin, Z. Y. Wang, Y. Wang, C. G. Di, K. Xiao, X. M. Chen, W. F. Qia, B. Zhang, G. Yu, W. P. Hu, D.B. Zhu, *Adv. Funct. Mater.* **2006**, *16*, 426.
[34] J. Youn, M.-C. Chen, Y.-J. Liang, H. Huang, R. P. Ortiz, C. Kim, C. Stern, T.-S. Hu, L.-H. Chen, J.-Y. Yan, A. Facchetti, T. J. Marks, *Chem. Mater.* **2010**, *22*, 5031.
[35] P.-Y. Huang, L.-H. Chen, C. Kim, H.-C. Chang, Y.-j. Liang, C.-Y. Feng, C.-M. Yeh, J.-C. Ho, C.-C. Lee, M.-C. Chen, *ACS Appl. Mater. Interfaces* **2012**, *4*, 6992.
[36] P.-Y. Huang, L.-H. Chen, Y.-Y. Chen, W.-J. Chang, J.-J. Wang, K.-H. Lii, J.-Y. Yan, J.-C. Ho, C.-C. Lee, C. Kim, M.-C. Chen, *Chem. Eur. J.* **2013**, *19*, 3721.
[37] J. Youn, S. Kewalramani, J. D. Emery, Y. Shi, S. Zhang, H.-C. Chang, Y.-j. Liang, C.-M. Yeh, C.-Y. Feng, H. Huang, C. Stern, L.-H. Chen, J.-C. Ho, M.-C. Chen, M. J. Bedzyk, A. Facchetti, T. J. Marks, *Adv. Funct. Mater.* **2013**, *23*, 3850.
[38] Devices with Au as the S/D electrode material had an injection barrier of holes into the HOMO of the M-BTDT (ca. 0.53 eV) that was similar to the barrier into the LUMO of C_{60} (ca. 0.5 eV). This injection barrier could be decreased significantly, however, through the formation of strong interface dipoles and metal doping at the Au–C_{60} interface. S. C. Veenstra, A. Heeres, G. Hadziioannou, G. A. Sawatzky, H. T. Jonkman, *Appl. Phys. A.* **2002**, *75*, 661.
[39] M.-C. Chen, C. Kim, S.-Y. Chen, Y.-J. Chiang, M.-C. Chung, A. Facchetti, T. J. Marks, *J. Mater. Chem.* **2008**, *18*, 1029.
[40] High threshold voltages of ambipolar transistors in this study could probably be due to high contact resistance between semiconductor energy levels and work function of electrode (Au). Employing asymmetric electrodes (as in the case of single component ambipolar transistor) might be one way, although this would demand an additional deposition step. Furthermore, employing interlayer with appropriate energy level between electrode and semiconductor might be another way to decrease the contact resistance and to enhance the electrical performance of the devices. C.-W. Chu, S.-H. Li, C.-W. Chen, V. Shrotriya, Y. Yang, *Appl. Phys. Lett.* **2005**, *87*, 193508.